*J. Fluid Mech.* (1969), *vol.* 35, *part* 2, *pp.* 353–368
*Printed in Great Britain*



# Velocity gradients at the wall for flow around a cylinder at Reynolds numbers from $5\times10^3$ to $10^5$

By JAIME S. SON† AND THOMAS J. HANRATTY

Department of Chemistry and Chemical Engineering, University of Illinois, Urbana, Illinois

(Received 22 July 1968)

Electrochemical techniques have been used to measure the velocity gradients at the surface of a cylinder for Reynolds numbers from $5\times10^3$ to $10^5$. This is a companion study to that already reported by Dimopoulos & Hanratty (1968) for a Reynolds number range of 60–360. The use of a specially designed sandwich electrode enabled the direction of the velocity gradient as well as its magnitude to be measured. Of particular interest is the region of definite length after separation where the velocity gradient is negative, followed by an ill-defined region where the flow moves in the positive direction. Still farther downstream the direction of flow changes with time in an irregular fashion. The measured velocity gradients prior to separation are described satisfactorily by boundary-layer theory. The presence of a splitter plate in the rear of the cylinder eliminates periodic fluctuations in the wake and has a significant effect on the boundary layer prior to separation.

## 1. Introduction

This paper describes the second part of an investigation of the flow around a cylinder in which electrochemical techniques are used to measure the velocity gradients at the solid boundary. Dimopoulos & Hanratty (1968) used a cylinder of 1 in. diameter and covered a range of Reynolds numbers, $R$, between 60 and 360. The results now being presented were obtained for $5000 \leqslant R \leqslant 100{,}000$ using cylinders with diameters 1·500, 1·004 and 0·754 in.

The technique used is the mass transfer analogue of the thermal meter suggested by Ludweig (1949). A chemical reaction is carried out on the surface of a small electrode embedded in the wall. The electrochemical cell is operated under conditions that the mass transfer rate of the reacting species to the electrode surface is controlling the rate of reaction. The electrical current is then directly proportional to the average mass transfer coefficient $\langle k\rangle$. For the velocities used in this study natural convection at the electrode surface and axial diffusion can be neglected, so $\langle k\rangle$ can be related to the velocity gradient at the electrode surface, $\beta$, by the equation,

$$\langle k\rangle L/D = 0{\cdot}807Z^{\frac{1}{3}}, \tag{1}$$

† Present address: Shell Development, Emeryville, California.

where $D$ is the diameter of the cylinder, $L$ is the length of the electrode, and $Z = \beta L^2/D$.

Dimopoulos & Hanratty (1968) used a single round electrode, having a diameter of 0·020 in., or a single rectangular electrode 0·500 in. wide and 0·020 in. long. The cylinder was rotated in the test section so that the velocity gradient could be measured at different distances from the front stagnation point. These measurements only indicate the magnitude of the velocity gradient at the wall and not its direction. The location of the separation point was based on judging what would be a reasonable curve through the data points.

A much better method for determining the separation point was used for the measurements reported in this paper. A sandwich test electrode was developed which consisted of two platinum electrodes, 1 in. by 0·005 in., separated by 0·002–0·003 in. of insulation. If the flow is steady and the two electrodes are activated, one of the measurements will be significantly smaller than the other since it is in the wake of the other electrode. If the flow has large fluctuations, it is not easy to determine the flow direction from the time averaged signal. In this case one of the electrodes is operated as the test electrode. If the activation of the other electrode causes a sudden change in the signal from the test electrode, then the test electrode is in the wake of the second electrode. By using this technique it was possible to determine the separation point to within 1°, and also to obtain new insight into the wake structure close to the surface.

In the region before separation, the average velocity gradient was observed to have a periodic fluctuation superimposed upon it. In the rearward portions of the cylinder this periodic oscillation was obscured by the co-existence of random oscillations. The analysis of recordings of the signals enabled us to obtain values of the frequency of the periodic aspect of the wake motion in a range of Reynolds numbers where accurate measurements are not available.

Some experiments were performed with a splitter plate located in the wake of the cylinder, since it has been found by Roshko (1953) that the presence of a splitter plate eliminates the periodic aspect of wake motion. The differences of measurements of the velocity gradients for cylinders with or without a splitter plate show that the wake can significantly influence the boundary-layer regions in the front of the cylinder.

The only measurements of velocity gradients at the surface of a cylinder other than those by Dimopolous & Hanratty (1968) of which we are aware were obtained with surface tubes by Fage & Falkner (1931) and by Fage (1936) over a Reynolds number range of $10^5$ to $10^6$. Bellhouse & Schultze (1966) studied flow around a cylinder by a heated metallic film, but they did not calculate velocity gradients. A comparison of the skin friction measured by Fage & Falkner with the prediction of boundary-layer theory indicated fair agreement with their 6 in. cylinder and very poor agreement with their 2·5 in. cylinder. As indicated by Fage & Falkner, it is most likely that this lack of agreement is the result of inaccuracies in their measurements caused by the relatively large size of the surface tube compared to the thickness of the boundary layer. The results presented in this paper offer an opportunity of examining the accuracy of calculations based on boundary-layer theory. It is felt that the calculation of skin

friction from electrochemical measurements is more accurate than boundary-layer calculations based on measured pressure profiles, since the derivative of the pressure in the direction of flow is needed. It is found that boundary-layer theory does a reasonable job and that the shear stress distribution in the neighbourhood of the front stagnation point agrees with predictions that use an external flow given by the classical inviscid analysis.

## 2. Description of the experiments

The experiments were carried out in the flow tunnel shown in figure 1. The test section is a rectangular duct, 6 in. × 12 in. The cylinders were aligned with their axes parallel to the 6 in. side of the test section so that ratios of cylinder diameter

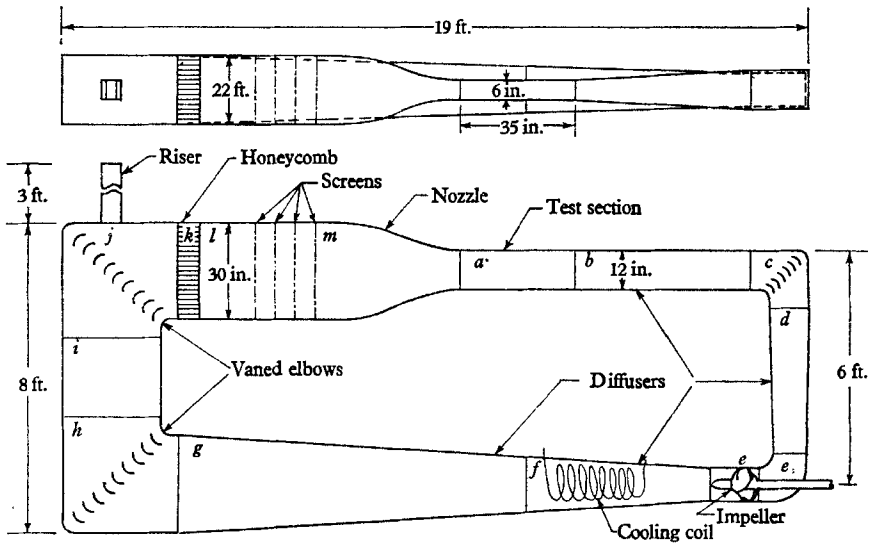


FIGURE 1. Water tunnel.

to section height of 1 : 16, 1 : 12 and 1 : 8 were used. The design of the tunnel is similar to what has been used in a number of other laboratories except that special precautions were taken in order to avoid contamination of the electrolyte. The materials that contact the electrolyte are either stainless steel or plastic. Provisions are made to purge the electrolyte with nitrogen before a run and to keep it in contact with an atmosphere of nitrogen during a run. The test section is preceded by a nozzle with a contraction ratio of 9 : 1. Four stainless steel screens separated from one another by 6 in. long blank sections are upstream of the nozzle. The first screen is 14 mesh and is constructed from wire with a diameter of 0·020 in. The other three are 20 mesh and have wire with a diameter of 0·012 in. The honeycomb that precedes the screens has rectangular cells which are 1 in. square and 6 in. long. Turning vanes are located in three of the elbows and an axial flow pump is used to circulate the fluid.

The electrolyte was 1 molar NaOH, 0·01 molar potassium ferricyanide and 0·01 molar potassium ferrocyanide. The temperature of the solution was main-

tained at 25 °C ± 0·05 °C by a controller and a cooling coil located in the diffuser following the pump outlet. The liquid in the riser at the top of the elbow preceding the test section was kept in contact with a nitrogen atmosphere. When not being used, the solution was stored in a black polyethylene tank having a capacity of 1000 gallons.

Velocity traverses made in the test section with Pitot tubes indicated that the profile was flat at the location, 12 in. from its inlet, where measurements were made. The velocity gradients at the surface of the cylinder were measured with a rectangular platinum electrode 0·015 in. long and 1 in. wide and with circular platinum electrodes having diameters of 0·0175–0·0211 in. As shown by Reiss (1960), the equivalent length of these circular electrodes to be used in (1) is equal to 0·82 times the diameter.

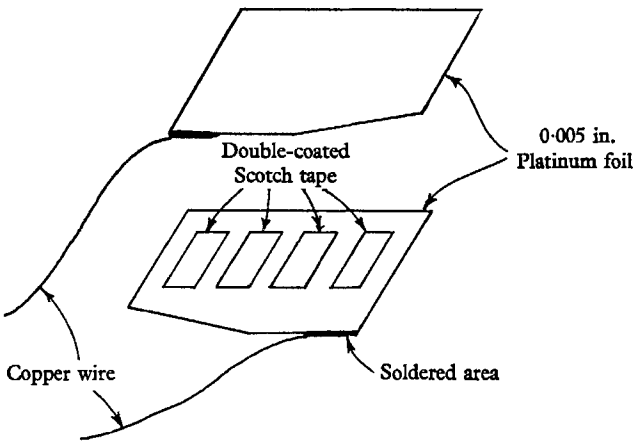


FIGURE 2. Fabrication of sandwich electrode.

The sandwiched test element was fabricated from two 1 in. × $\frac{1}{4}$ in. platinum foils, 0·005 in. thick. Copper wires were soldered to the longer edges in such a manner that when the two foils were glued together contact between the wire of one foil and the surface of the other was prevented (see figure 2). Four square pieces of double-coated Scotch tape were placed on one of the foils and epoxy resin was applied around them. The two foils were then pressed together in a machinists vice. After the epoxy had hardened the platinum foils were drawn through a slit in the surface of the test cylinder so that only about $\frac{1}{32}$ in. protruded on the outside surface of the cylinder. Prior to inserting the test element the slit had been filled with epoxy glue. After about 36 h the excess epoxy and platinum were removed with a small smooth file. The area was then sanded with progressively finer grades of emery paper. The copper lead wires were insulated from one another and brought through the centre of the tube to two separate circuits, both of which used a large platinum sheet located at the outlet of the test section as the reference electrode. These circuits were the same as those used by Mitchell & Hanratty (1966).

Before making a run the test cylinder was cleaned with a detergent and water by using a soft brush. After the washing, the cylinder was rinsed with deionized

water. Preliminary tests showed that the flow around the cylinder was symmetric. Therefore the front stagnation point was used as a reference point and was located as the minimum in the mass transfer rate. At high Reynolds numbers fluctuations were present at the front stagnation point so the flow rate had to be first reduced in order to locate the front stagnation point. The reference point determined in this manner agreed to within $\pm \frac{1}{4}$ degree with that determined from the alignment of the cylinder in the test section. The test electrode was located at different distances from the front stagnation point by rotating the test cylinder. Beyond 65° the test signal fluctuated so that it was necessary to integrate for a period of 3–5 min.

A more detailed account of the procedures and of the design of the equipment is given in a thesis by one of the authors (Son 1968).

## 3. Measured velocity gradients at the wall.

The measurements of the time averaged absolute values of the velocity gradients, $|\bar{\zeta}|$, at the wall of the cylinder have been made dimensionless with respect to the free-stream velocity, $u_\infty$, and the cylinder radius, $\frac{1}{2}d$. They are presented in figures 3–10 as a function of the angular distance from the front stagnation point. The Reynolds number used in the figures has been defined in terms of the diameter of the cylinder, $d$, and the free-stream velocity. The separation point, as determined by the sandwiched electrodes, is indicated with an arrow and the symbol $S$. The velocity gradient, $\zeta$, is positive in region $A$ and negative in region $B$. In the early part of region $C$ it is positive. However, over most of region $C$ it changes direction as time goes on. Measurements made with circular and rectangular electrodes are compared in figure 3 for a 1 in. cylinder at $R = 20{,}000$. The calculated values of $|\bar{\zeta}|$ for the two electrodes are within experimental error at locations before separation. After separation the values obtained from the rectangular electrodes were distinctly smaller than those obtained with the circular electrodes. This difference could result from depletion of ferricyanide ions in the neighbourhood of the electrode or from three-dimensional effects. Because of its larger size a significant amount of reaction occurs on the surface of the rectangular electrode. In regions after separation the flow over the electrode surface might not sweep the product of reaction downstream. Flow recirculation in these regions could therefore cause the concentration of ferricyanide ions to be somewhat smaller than in the fluid approaching the cylinder. This effect could be particularly important in region $B$. If the fluctuating flow is three-dimensional, there could be a considerable amount of averaging of the signal over the surface of the rectangular electrode. It was therefore felt that measurements made with the circular electrodes give a more accurate estimate of the local value of $|\bar{\zeta}|$, and all of the results presented were obtained from electrodes with this geometry.

There is some uncertainty as to the meaning of the measurements in region $C$ and very near $S$ because the equation used to calculate the velocity gradient at the wall is not accurate when it is zero. Since the flow in $C$ is changing direction, there are occasions when the velocity gradient is close to zero. Therefore the

calculation of $|\bar{\zeta}|$ from the time averaged mass transfer measurements in this region is open to question. At the separation point a finite current is measured even though $\zeta = 0$.

The ratio of the diameter of the cylinder to the height of the test section, $d/h$, was varied from 0·062 to 0·125. As shown in figure 3 the measured velocity gradients are independent of blockage effects over the range of $d/h$ investigated.

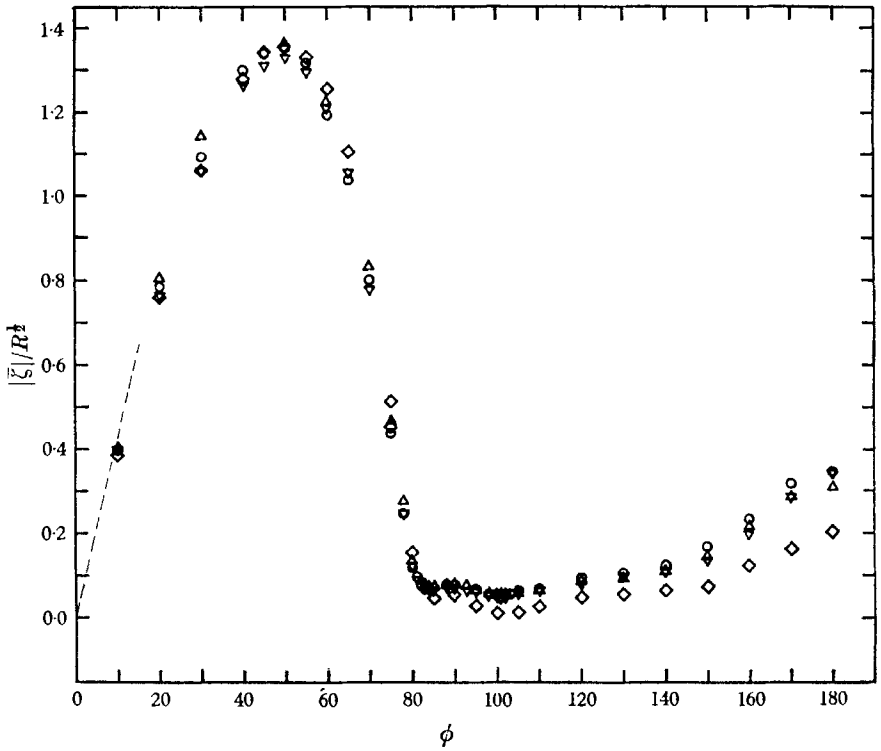


FIGURE 3. Effect of channel walls and of electrode design on the wall-velocity gradient measurements. $R$ = 20,000; △, ¾ in. cylinder, 27-gauge electrode, $d/h$ = 0·062. △; 1 in. cylinder, 25-gauge electrode, $d/h$ = 0·083; ○, 1½ in. cylinder, 25-gauge electrode, $d/h$ = 0·125; ◇, 1 in. cylinder, 0·0157 in. × 1 in. electrode, $d/h$ = 0·083.

The effect of a splitter plate at the rear of the cylinder is shown in figures 4 and 6. The extent of the regions $A$, $B$, $C$ is slightly affected. Of particular interest are the significantly smaller values of the velocity gradient obtained prior to separation when a splitter plate is used. Apparently the splitter plate causes the wake to be fatter so that the flow external to the boundary layer is better described by the inviscid solution for an object of somewhat different dimensions than the cylinder being studied.

The separation angles, measured from the rear of the cylinder, are presented in figure 11. It is seen that they increase from a value of 86° at $R$ = 5000 to a value of 102° at $R$ = 100,000. The presence of a splitter plate causes a slight increase in the angle of separation. It is to be noted that the measurements of the separation

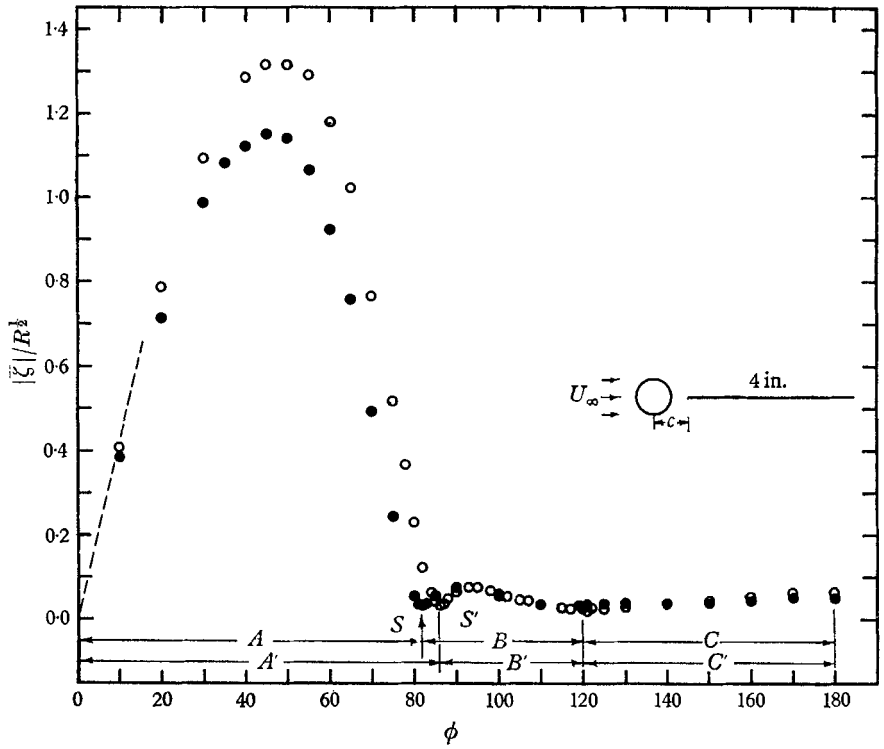


FIGURE 4. Effect of a splitter plate on the wall-velocity gradient distribution, $R = 5000$, $\frac{3}{4}$ in. cylinder, 27-gauge electrode, $d/h = 0{\cdot}062$. ○, no splitter plate; ●, with 4 in. splitter plate, $c/d = 1$.

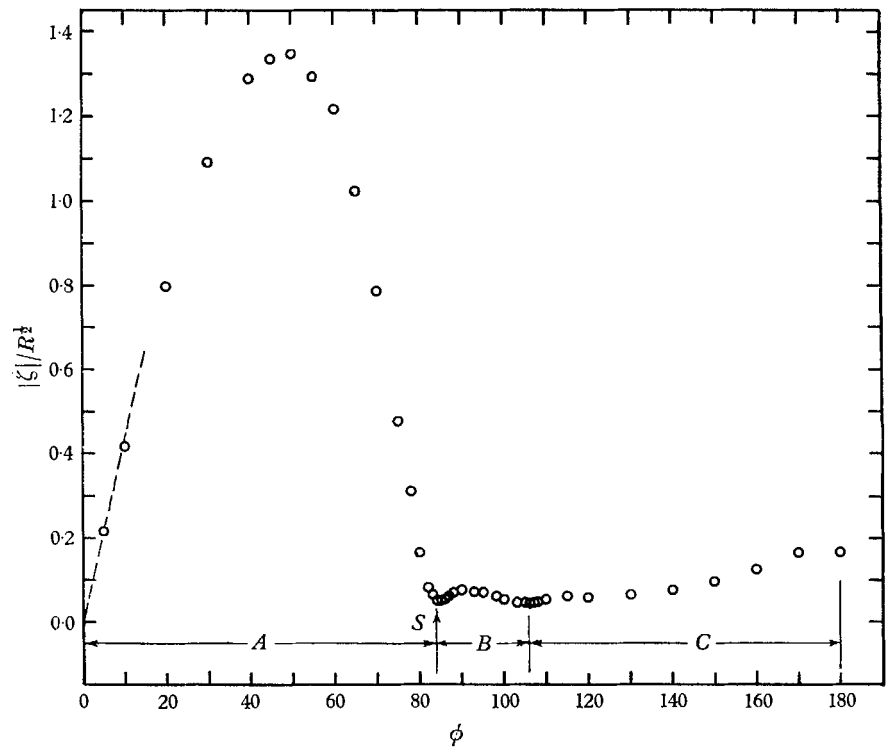


FIGURE 5. Normalized wall-velocity gradient distribution, $R = 10{,}000$, $\frac{3}{4}$ in. cylinder, $d/h = 0{\cdot}062$, 27-gauge electrode.

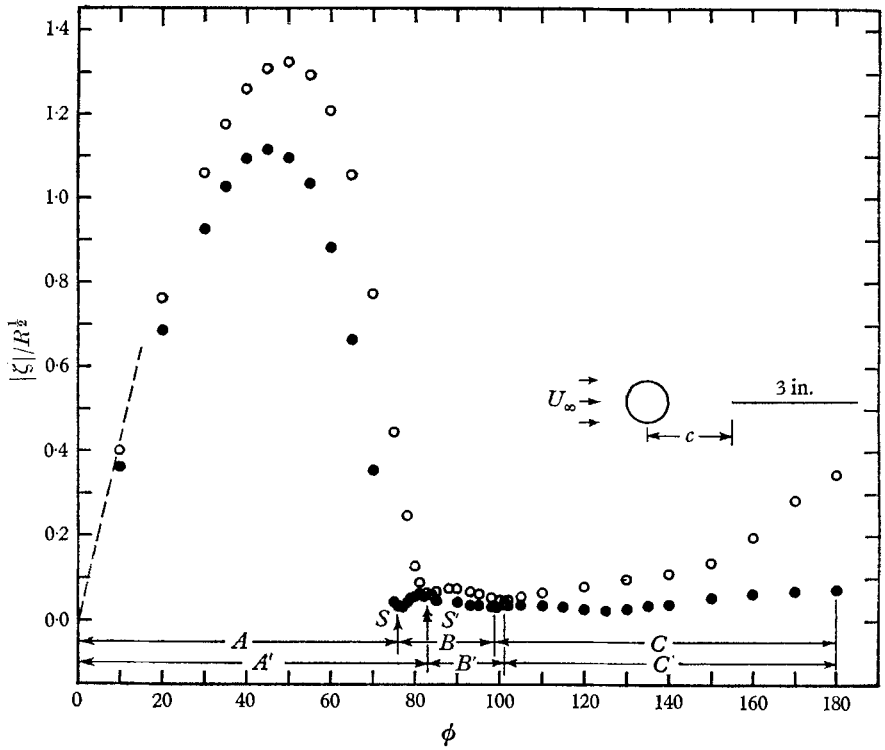


FIGURE 6. Effect of a splitter plate on the wall-velocity gradient distribution, $R$ = 20,000, 1 in. cylinder, 25-gauge electrode, $d/h$ = 0·083. ○, no splitter plate; ●, with 3 in. splitter plate, $c/d$ = 2.

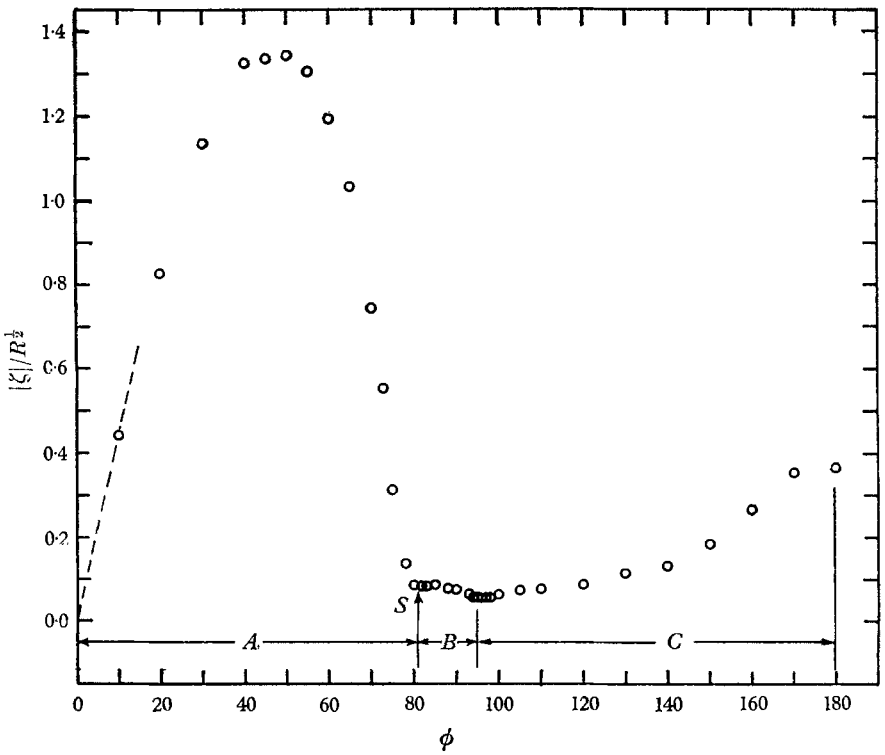


FIGURE 7. Normalized wall-velocity gradient distribution, $R$ = 40,000, $\frac{3}{4}$ in. cylinder, $d/h$ = 0·062, 27-gauge electrode.

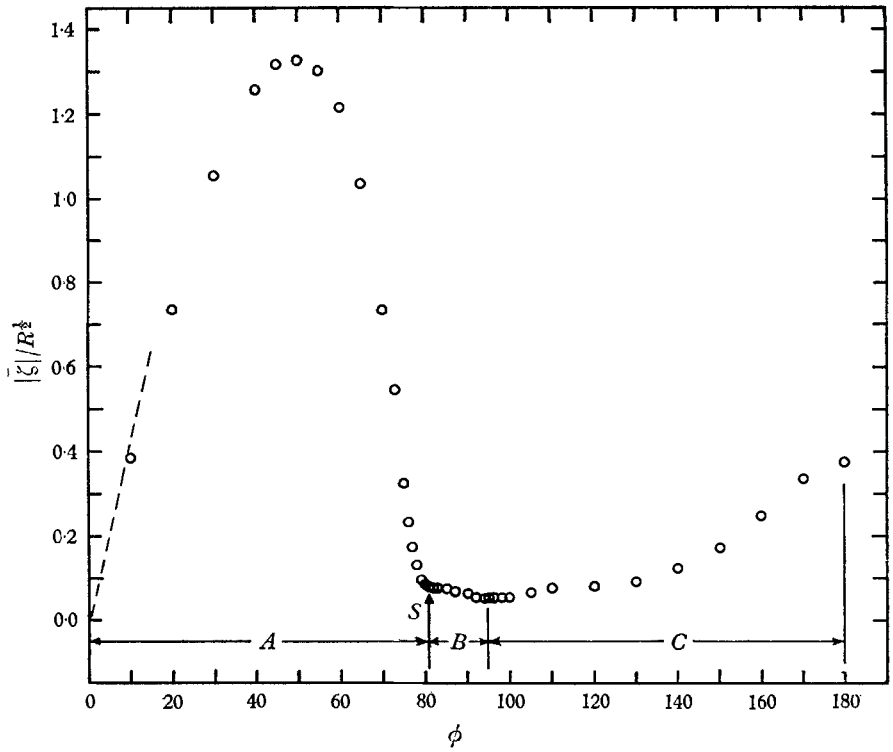


FIGURE 8. Normalized wall-velocity gradient distribution, $R$ = 50,000, 1 in. cylinder, $d/h$ = 0·083, 25-gauge electrode.

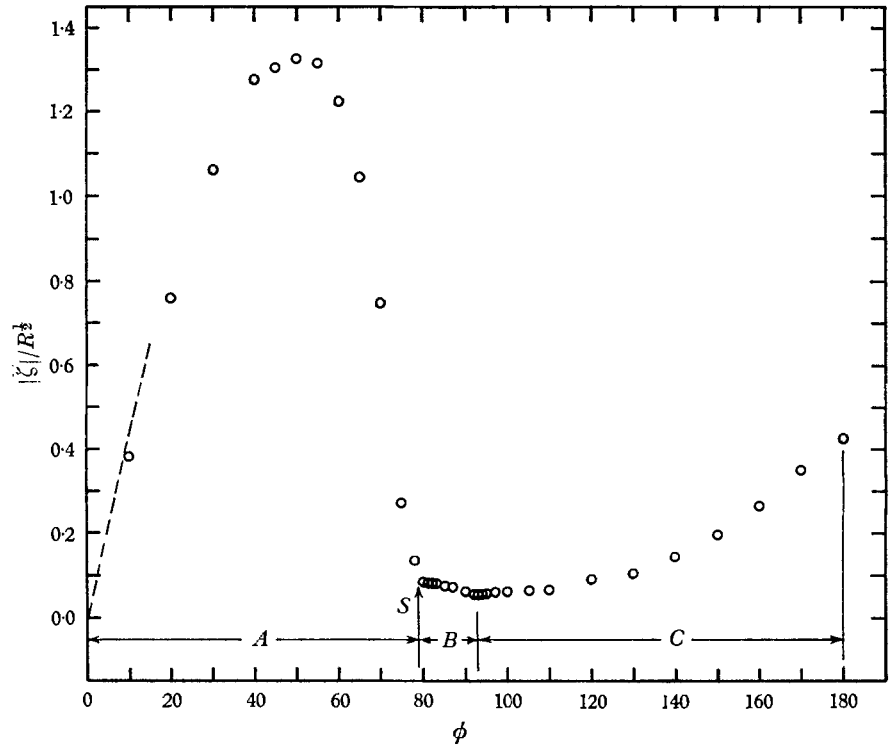


FIGURE 9. Normalized wall-velocity gradient distribution, $R$ = 70,000, 1 in. cylinder, $d/h$ = 0·083, 25-gauge electrode.

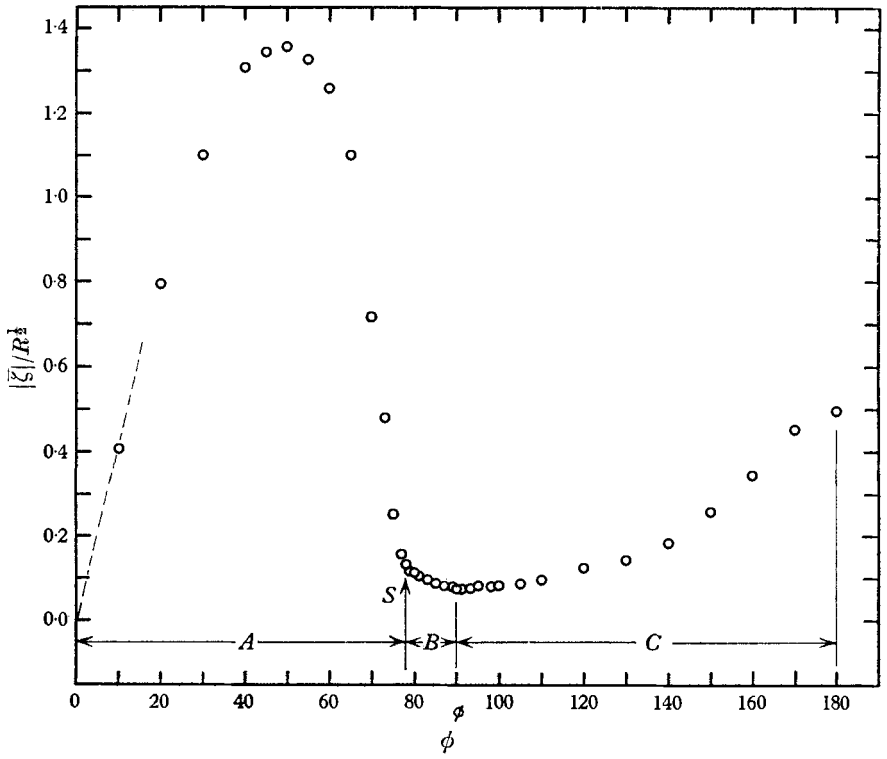


FIGURE 10. Normalized wall-velocity gradient distribution, $R$ = 100,000, $1\frac{1}{2}$ in. cylinder, $d/h$ = 0·125, 25-gauge electrode.

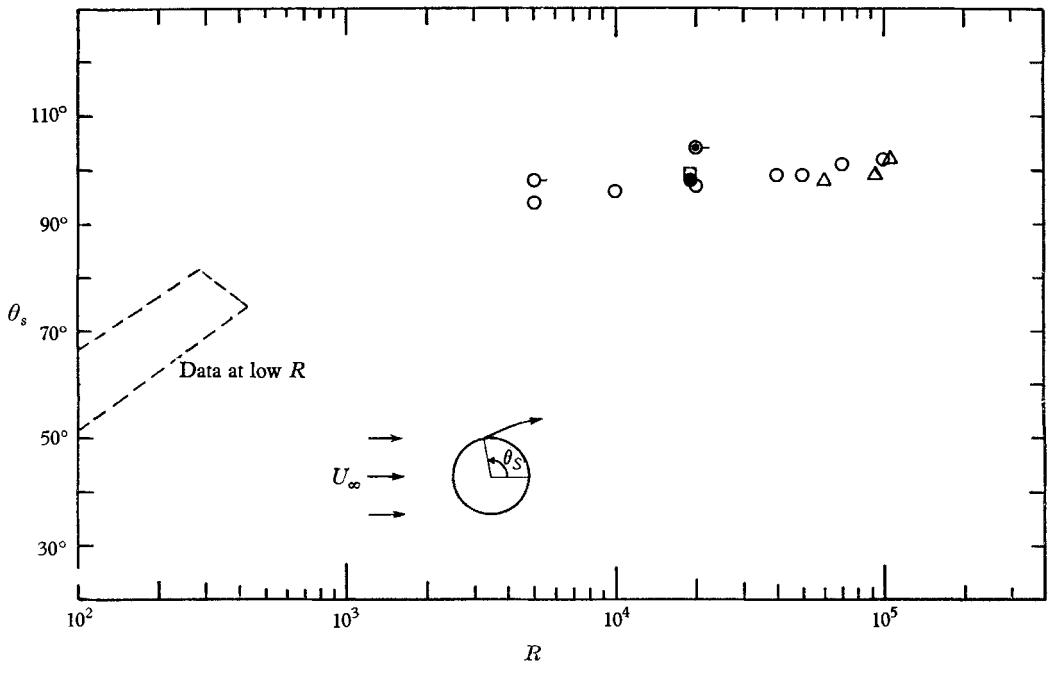


FIGURE 11. Effect of Reynolds number on the angle of separation. ○, this study; ○–, this study, with splitter plate, $c/d$ = 1; ⊙–, this study, with splitter plate, $c/d$ = 2; □, Hiemenz (1911); △, Fage & Falkner (1931); ●, boundary-layer solution, Hiemenz's pressure distribution.

angle reported by Hiemenz (1911) and by Fage & Falkner (1931) are in good agreement with the ones reported in this paper.

One possible explanation of the region $B$ designated in figures 3–10 is the existence of a separation bubble. The length of this region in degrees, $\theta_v$, decreases

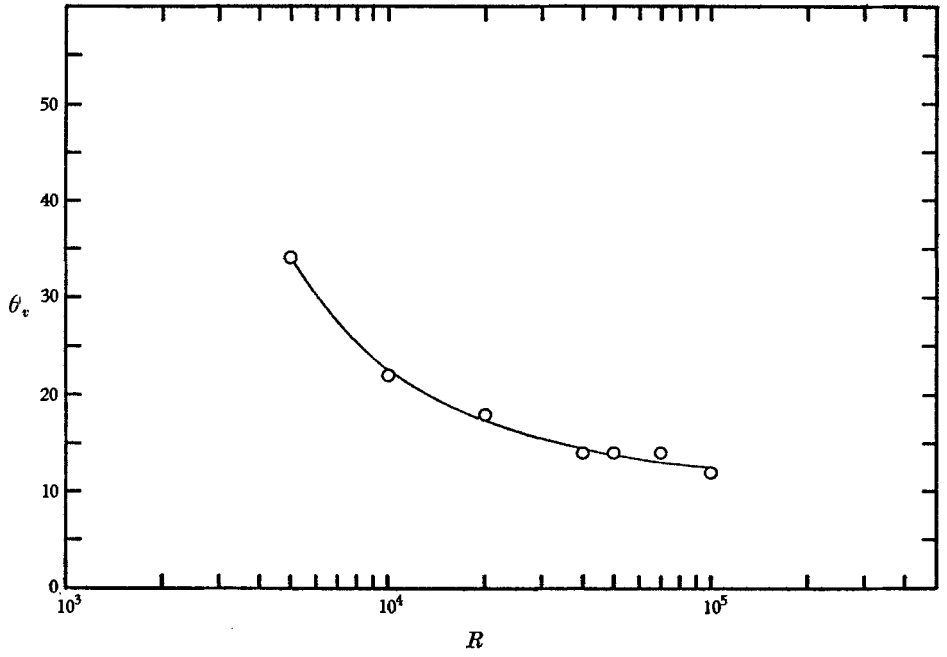


FIGURE 12. Effect of Reynolds number on the length of the secondary vortex.

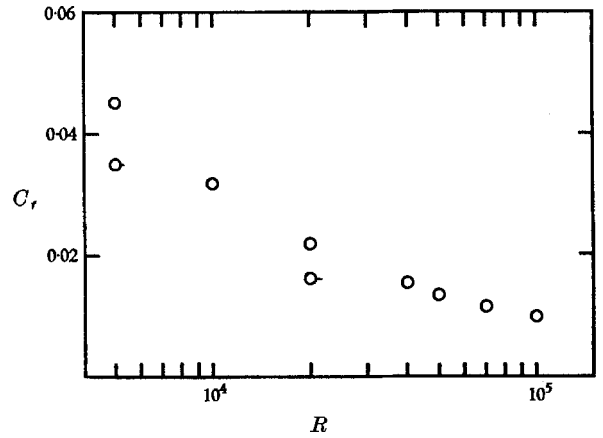


FIGURE 13. Skin-friction drag. ○–, with splitter plate; ○, without splitter plate.

with increasing Reynolds number, as indicated in figure 12. It is of interest to note that at large Reynolds numbers the end of region $B$ occurs approximately at 90°.

The contribution of the skin friction to the drag on the cylinder cannot be calculated exactly from the measurements since the contribution of region $C$

cannot be determined. If it is assumed that this is small, then an estimate of skin drag can be obtained by integrating the measurements for regions $A$ and $B$. These estimates, presented in figure 13, are in reasonable agreement with values calculated as the difference between the total drag and the form drag (Goldstein 1938).

## 4. Comparison with boundary-layer theory

All of the measured velocity gradients prior to separation are presented in figure 14. As predicted by boundary-layer theory, measurements at different Reynolds numbers collapse on a single curve when the dimensionless velocity gradient is normalized with respect to $\sqrt{R}$.

According to the potential flow solution the velocity external to the boundary layer is given by $U = 4xu_\infty/d$ in the neighbourhood of the front stagnation point where $x$ is the distance along the cylinder surface. The boundary-layer solution based on this external flow is given by Schlichting (1960) and is indicated by the

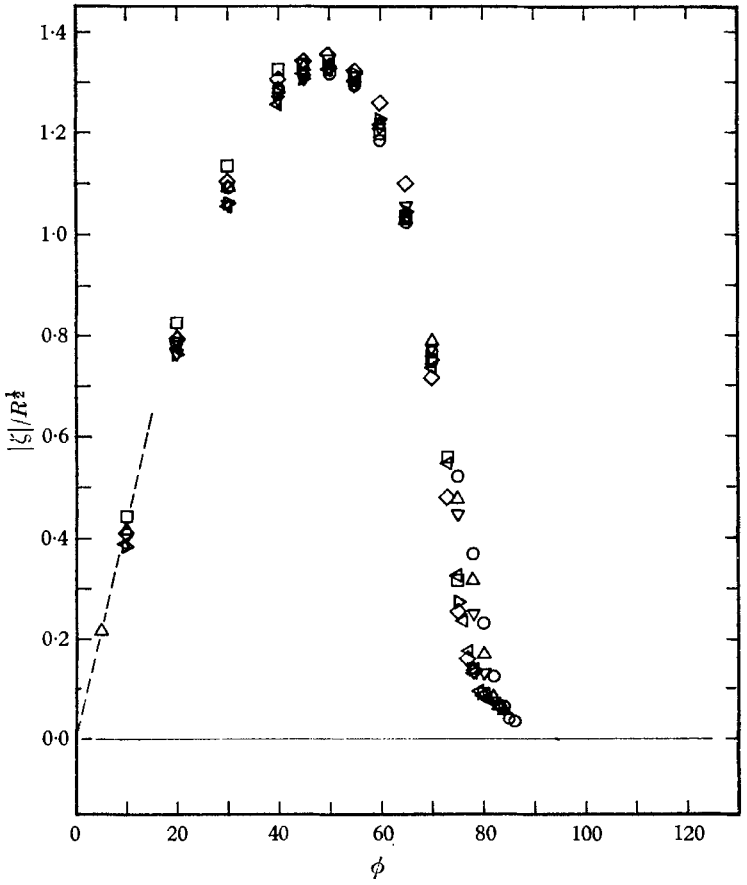


FIGURE 14. Effect of Reynolds number on the wall-velocity gradient distribution. ○, $R$ = 5000; △, $R$ = 10,000; ▽, $R$ = 20,000; □, $R$ = 40,000; ◁, $R$ = 50,000; ▷, $R$ = 70,000; ◇, $R$ = 100,000; ———, boundary-layer solution (potential flow).

dotted line in figures 3–10. It is seen that the measured velocity gradients in the neighbourhood of the front stagnation point are in good agreement with this solution when no splitter plate is located behind the cylinder.

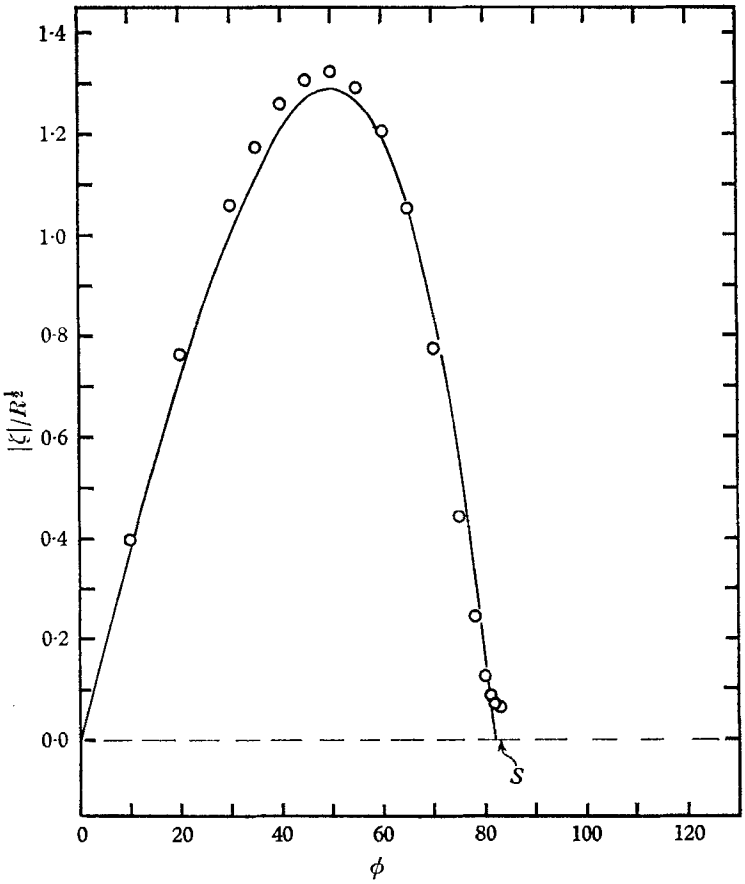


FIGURE 15. Comparison between boundary-layer calculations and measurements. ○, this study, $R$ = 20,000; ———, boundary-layer solution, $R$ = 19,000.

The prediction of the complete profile from boundary-layer theory requires rather accurate pressure measurements, and it can vary significantly with slight changes in the pressure profile. A calculation based on Hiemenz's pressure measurements at $R$ = 19,000 was carried out using the Blasius series (Schlichting 1960). A comparison between the calculation and measured velocity gradients at $R$ = 20,000 is shown in figure 15. Good agreement is obtained both for the location of the separation point and the variation of surface velocity gradient.

## 5. Flow fluctuations

Oscillograms of the voltage signals from the electrodes are shown in figures 16–19 (plates 1 and 2) for $R$ = 5000 and 20,000. These voltages are directly proportional to the current flowing in the circuit and $\bar{v}$ is the time averaged voltage.

Over the front portion of the cylinder the oscillations are sinusoidal and of constant frequency. The amplitude of these oscillations is quite large near the separation point. At, or near, the separation point irregular fluctuations are superimposed upon the sinusoidal ones. Farther from separation the fluctuations

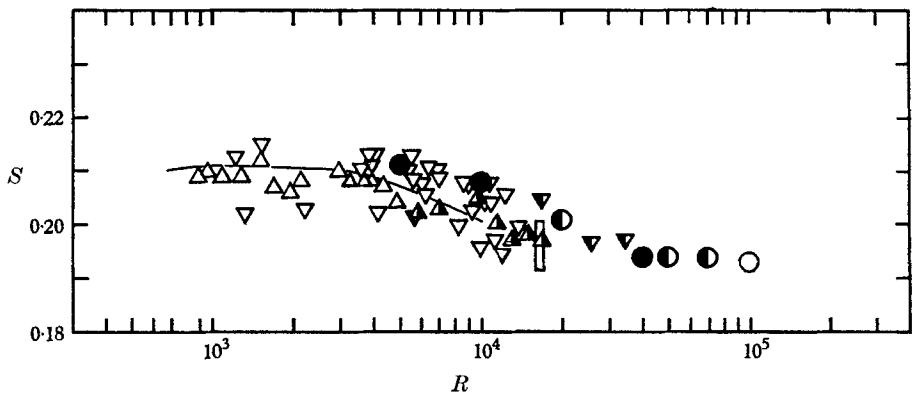


FIGURE 20. Strouhal number. This study: ●, $d/h = 0{\cdot}062$; ◐, $d/h = 0{\cdot}083$; ○, $d/h = 0{\cdot}125$. Roshko (1954): △, $d/h = 0{\cdot}012$; ▲, $d/h = 0{\cdot}043$. ——, Roshko (1953). Gerrard (1966): ▽, $d/h = 0{\cdot}012$; ▼, $d/h = 0{\cdot}05$; ▯, $d/h = 0{\cdot}05$, represents 22 points.

become more irregular, and both the amplitude and frequency increase. When a splitter plate is located behind the cylinder, the regular sinusoidal fluctuations are no longer present. The frequency, $f$, of the regular fluctuations is plotted in figure 20 as a Strouhal number, $S = fd/u_\infty$. These results are in good agreement with measurements of flow fluctuations in the wake by Roshko (1954) and Gerrard (1966). The present results indicate a slight decrease in the Strouhal number between $R = 5000$ and $R = 100{,}000$.

## 6. Flow pattern

The measurements of the velocity gradients at the wall of a cylinder without a splitter plate are similar to some of the computer computations presented by Thoman & Szewczyk (1966). A possible picture of the flow pattern is indicated in figure 21. The region $B$ is interpreted as a small relatively stationary secondary vortex after the separation point. The gross wake structure is pictured as oscillating between that pictured in figure 21 (*a*) and that in figure 21 (*b*). It is to be noted that according to this model the flow immediately after the secondary vortex is in the positive direction and that farther downstream it alternates its direction with time. In the rear of the cylinder highly complicated three-dimensional flow fluctuations are superimposed on this gross structure.

Some support for such a model is obtained from visual studies that were conducted. Dye was injected into the flow stream from a small hole located on the surface of the cylinder. The paths taken by the dye streamers when the injection point was at different circumferential positions at $R = 5000$ is shown in figure 22. The separated dye streamer was very distinct and was observed to roll into

vortices which were shed immediately. When the dye orifice was located at the front stagnation point, the dye divided into two streamers on opposite sides of the cylinder. The vortices formed by these streamers were shed alternately. The separated dye streamer oscillated gently in the $(X, Y)$-plane and in the $(X, Z)$-plane. The former is believed to be due to vortex shedding while the latter is due

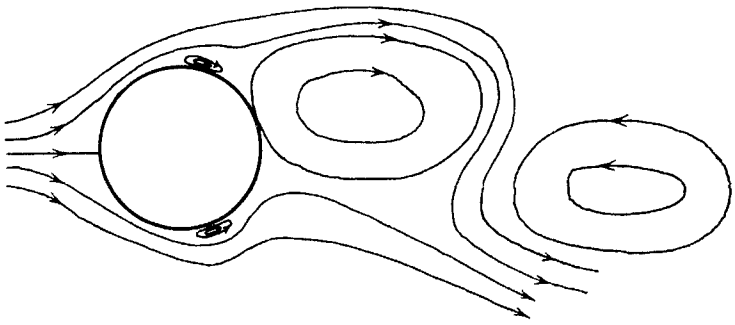

(*a*)

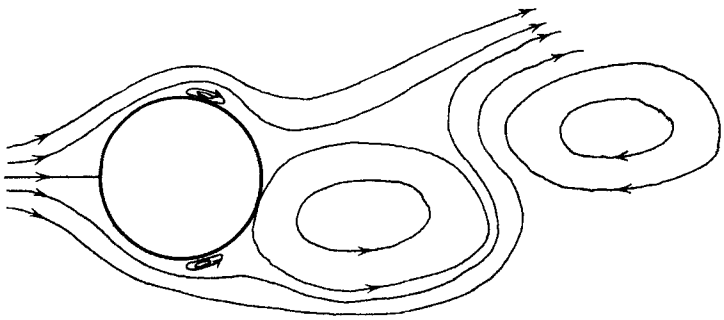

(*b*)

FIGURE 21. Sketch of the proposed flow pattern.

to three-dimensional effects. When the dye was injected at the wall in region $B$ it moved backwards before separating as indicated in figure 22 (*b*). When injected in the rear of the cylinder, its direction alternated both in the $X$-direction and in the $Z$-direction as shown in figure 22 (*c*) and 22 (*e*).

The dye patterns observed at $R = 20{,}000$ differed from those for $R = 5000$ in that the separated dye streamer rolled into vortices at a position closer to the surface of the cylinder. The formation and the shedding of the vortices was very rapid. The oscillation frequency of the separated dye streamer was much larger.

The only important difference observed when a splitter plate was placed behind the cylinder was that the separated dye streamer did not roll into a vortex but diffused immediately and mixed with the turbulent fluid.

Support for this research was received from the Air Force Office of Scientific Research under Grant AFOSR 547 and from the donors of the Petroleum Research Fund, administered by the American Chemical Society.

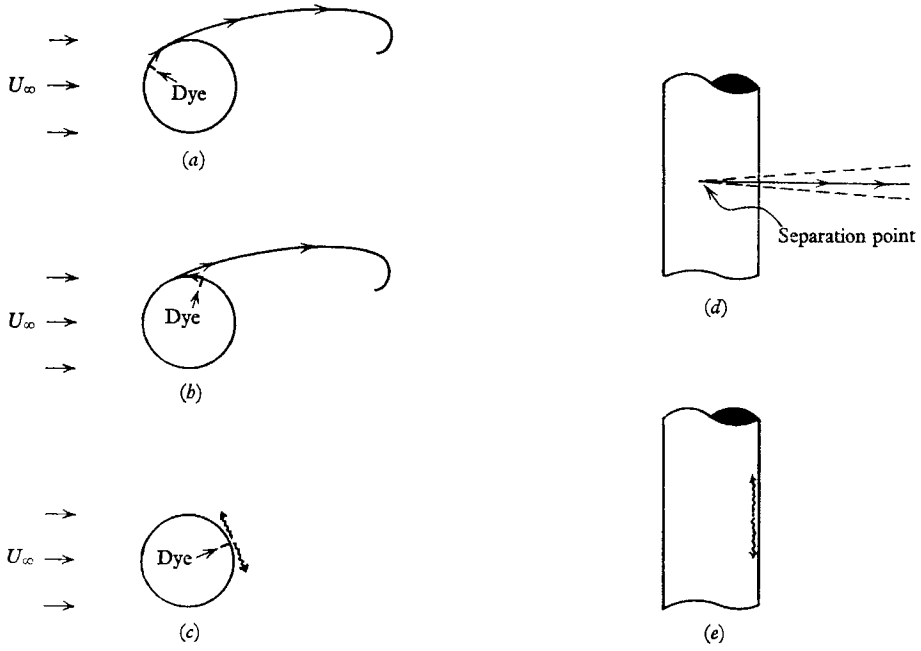


FIGURE 22. Dye pattern around a circular cylinder, $N_{Re} = 5000$. (*a*) Region *A*. (*b*) Region *B*. (*c*) Region *C*. (*d*) Top view, (*X*, *Z*)-plane, of separated dye streamer in (*a*) and (*b*). (*e*) Top view, (*X*, *Z*)-plane, of separated dye streamer in (*c*).

## REFERENCES

BELLHOUSE, B. J. & SCHULTZ, B. L. 1966 *J. Fluid Mech.* **24**, 379.

DIMOPOULOS, H. D. & HANRATTY, T. J. 1968 *J. Fluid Mech.* **33**, 303.

FAGE, A. 1936 *A.R.C.R. & M.* no. 1765.

FAGE, A. & FALKNER, V. M. 1931 *A.R.C.R. & M.* no. 1369.

GERRARD, J. H. 1966 *J. Fluid Mech.* **25**, 401.

GOLDSTEIN, S., ed. 1938 *Modern Developments in Fluid Mechanics*, vol. II. Oxford University Press.

HIEMENZ, K. 1911 *Dingl. Polytechn. J.* **326**, 321.

LUDWEIG, H. 1949 *N.A.C.A. Tech. Memo.* no. 1284.

MITCHELL, J. E. & HANRATTY, T. J. 1966 *J. Fluid Mech.* **26**, 199.

REISS, L. P. 1960 M.S. thesis, University of Illinois, Urbana.

ROSHKO, A. 1953 *N.A.C.A. Tech. Note.* no. 2913.

ROSHKO, A. 1954 *N.A.C.A. Tech. Note* no. 3169.

SCHLICHTING, H. 1960 *Boundary Layer Theory*, 4th ed. New York: McGraw-Hill.

SON, S. J. 1968 Ph.D. thesis, University of Illinois, Urbana.

THOMAN, D. C. & SZEWEZYK, A. A. 1966 *Heat Transfer and Fluid Mechanics Laboratory, University of Notre Dame. Tech. Rep.* 66-14.

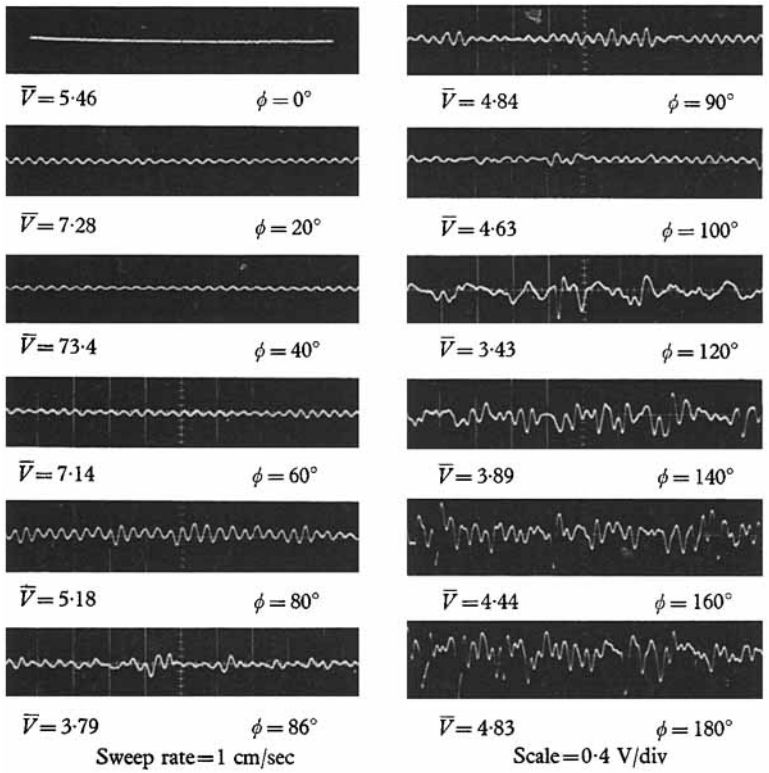


FIGURE 16. Oscillograms of the electrode voltage signals around the $\frac{3}{4}$ in. cylinder without a splitter plate. $R$ = 5000.

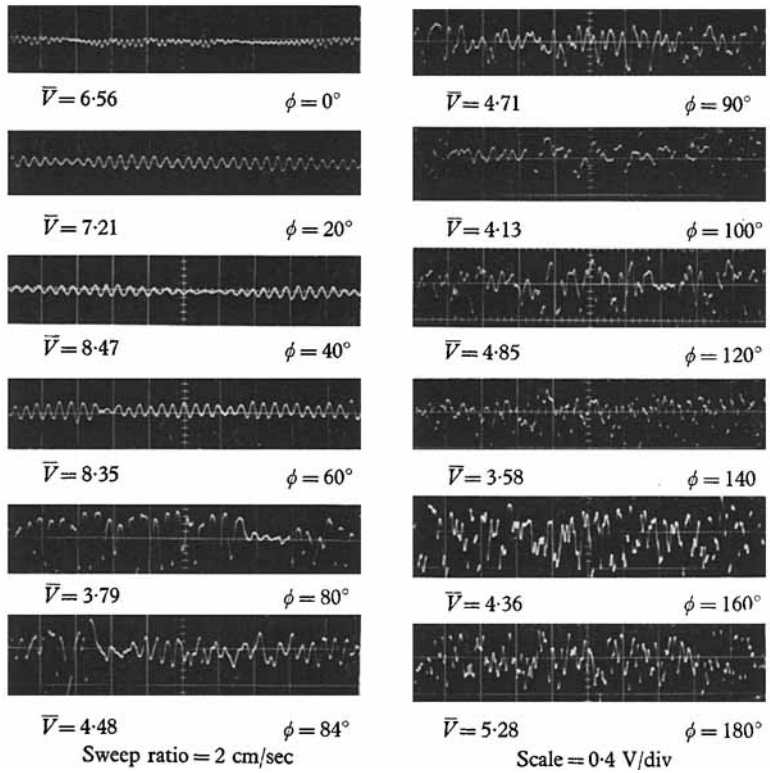


FIGURE 17. Oscillograms of the electrode voltage signals around the 1 in. cylinder without a splitter plate. $R$ = 20,000.



(*Facing p.* 368)

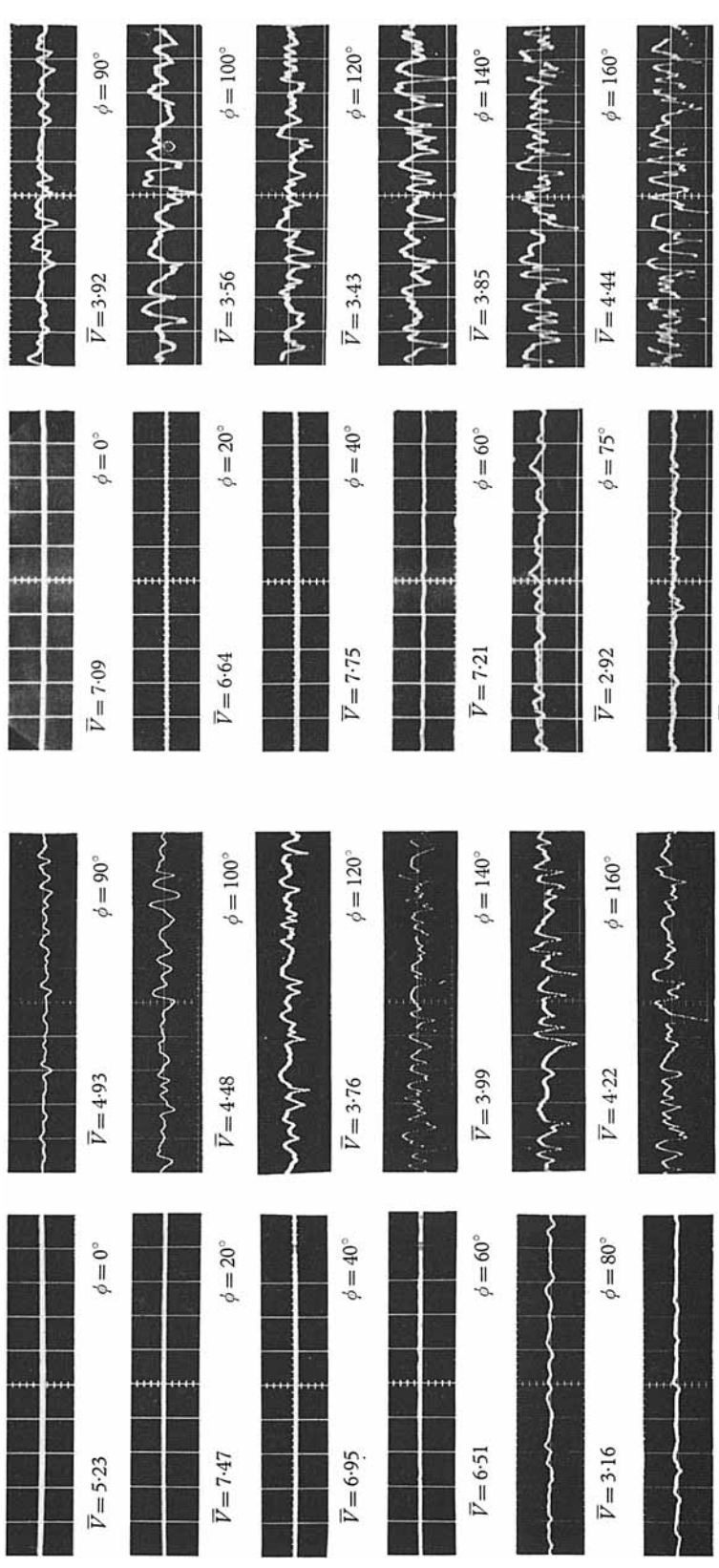


FIGURE 18. Oscillograms of the electrode voltage signals around the 3 ft. 4 in. cylinder with a 4 in. splitter plate, $c/d = 1$. $R = 5000$.




FIGURE 19. Oscillograms of the electrode voltage signals around the 1 in. cylinder with a 3 in. splitter plate, $c/d = 2$. $R = 20{,}000$.